
Article:
Wang, G., Lu, Z. orcid.org/0000-0002-9967-5221, Zhang, Z. et al. (3 more authors) (2019) Electric field-induced irreversible relaxor to ferroelectric phase transformations in Na0.5Bi0.5TiO3-NaNbO3 ceramics. Journal of the American Ceramic Society, 102 (12). pp. 7746-7754. ISSN 0002-7820

https://doi.org/10.1111/jace.16676

Electric field-induced irreversible relaxor to ferroelectric phase transformations in $Na_{0.5}Bi_{0.5}TiO_3$-$NaNbO_3$ ceramics

Ge Wang,[a,b] Zhilun Lu,[a] Zhenbo Zhang,[b] Antonio. Feteira,[c] Chiu. C. Tang,[d] David. A. Hall[b]

a. Department of Materials Science and Engineering, University of Sheffield, Sheffield S1 3JD, UK.

b. School of Materials, University of Manchester, Manchester, M13 9PL, UK.

c. Materials and Engineering Research Institute, Sheffield Hallam University, Sheffield S1 1WB, UK.

d. Diamond Light Source Ltd, Harwell Science and Innovation Campus, Didcot, OX11 0DE, UK.

Corresponding email: david.a.hall@manchester.ac.uk

Abstract

(1-x)$Na_{0.5}Bi_{0.5}TiO_3$-x$NaNbO_3$ (x=0.02, 0.04, 0.06 and 0.08) ceramics were fabricated by solid state reaction. High-resolution synchrotron x-ray powder diffraction (SXPD) data, coupled with macroscopic electromechanical measurements, reveal the occurrence of an electric field-induced irreversible crystallographic transformation for x=0.02 and 0.04, from a pseudo-cubic non-ergodic relaxor to a rhombohedral or coexisting rhombohedral-tetragonal long range-ordered ferroelectric phase respectively. The highest unipolar electrostrain, corresponding to an effective longitudinal piezoelectric strain coefficient of approximately 340 pm V^{-1}, was obtained for x=0.04; this effect is attributed to enhanced domain switching as a result of the co-existing rhombohedral and tetragonal phases for this composition, which is critical for piezoelectric actuator applications.

Keywords: sodium bismuth titanate, phase transformation, high-resolution synchrotron x-ray diffraction, ferroelectric, relaxor ferroelectric

1. Introduction

For many decades, electromechanical devices such as actuators, transducers and sensors have been manufactured using lead zirconate titanate (PZT) ceramics, with compositions near a so-called *morphotropic phase boundary* (MPB). Coexistence of rhombohedral and tetragonal crystal symmetries at the MPB leads to large piezoelectric and electromechanical coupling coefficients.[1] Nevertheless, confirmed legislation restricting the use of lead in electronics due its hazardous and toxic nature demands the substitution of PZT by Pb-free alternatives. Indeed, significant research has been conducted in order to develop Pb-free piezoelectrics that may be suitable to replace PZT in many technological applications.[2]

First reported in 1961, $Na_{0.5}Bi_{0.5}TiO_3$ (NBT) has become one of the most popular candidates to replace PZT because of its high remnant polarization and electric field-induced strain.[3] Undoped NBT ceramics exhibit a large coercive field (E_c),[4] but, due to interest in electromechanical actuator applications, several NBT-based solid solutions been developed such as NBT-0.06$BaTiO_3$-$K_{0.5}Na_{0.5}NbO_3$ (NBT-BT-KNN). Such materials tend to exhibit lower E_c values but still provide large electric field induced strains.[5, 6]. Recently, NBT-based solid solutions such as NBT-0.08BT-$NaNbO_3$(NN) have also been explored for dielectric energy storage applications.[7] The temperature-dependence relative permittivity of NBT-based materials is often marked by a significant frequency dispersion, which is due to the presence of polar nano-regions (PNRs), commonly found in other lead [8-14] and lead-free [15-21] relaxor ferroelectrics (RFs). NBT-based solid solutions, such as NBT-0.07BT and NBT-x$KNbO_3$ (NBT-xKN) (x=0.01-0.09) are often reported to have a pseudo-cubic structure, commensurate with a RF. [22, 23] Interestingly, the structure of unmodified NBT has been described as

macroscopically rhombohedral with localised nanoscale monoclinic regions. [24, 25]

It has been shown that many NBT-based ceramics exhibit improved electrostrain as a result of an electric field-induced phase transformation from a non-ergodic RF to a metastable ferroelectric (FE) state. This is accompanied by a transformation from pseudo-cubic to distinctive lower-symmetry structures. For example, an electric field-induced structural transformation from pseudo-cubic to mixed rhombohedral and tetragonal phases was found in NBT-0.07BT by Daniel [23], generating a high electric field-induced strain of 0.42% in single crystal form. [26] Furthermore, the addition of 1-2% KNN to NBT-BT leads to a higher polarisation and an even higher electric field-induced strain ~ 0.49%, as found by Jo [27] in bulk ceramics. In the related NBT-0.2$K_{0.5}Bi_{0.5}TiO_3$(NBT-KBT) solid solution, a structural transformation from pseudo-cubic to a combination of rhombohedral and tetragonal symmetries was identified by Royles et al [28] using "*in-situ*" synchrotron x-ray diffraction. Recently, an electric-field induced structural transformation from pseudo-cubic to rhombohedral was also reported in the (1-x)NBT-xKN solid solutions with x=0.01-0.05.[22]. This transformation was also found to be reversible upon heating.[29]

$NaNbO_3$ (NN) is generally accepted to be an anti-ferroelectric (AFE) compound with orthorhombic structure.[30] Nevertheless, refinement of high-resolution neutron diffraction data has revealed a FE monoclinic structure.[31] Recently, Jung et al [32] proposed using pure NN in piezoelectric nano-devices, such as a piezoelectric nano-generator. Moreover, $NaNbO_3$ is reported to be a promising lead-free material for high energy density ceramic capacitors. By adding a small amount of Bi_2O_3, an ultrahigh energy storage efficiency of 85.4% and energy density of 4.03 J cm^{-3} at 250 kV cm^{-1} was reported by Zhou *et al*. [33] Overall, NN is regarded

as an attractive lead-free piezoelectric end-member, particularly in binary or ternary solid solutions such as (Na, K, Li)NbO_3.[34, 35] Li *et al* investigated the NBT-xNN solid solution and identified a rhombohedral structure with x=0-0.06, which changes to pseudo-cubic when x increases to 0.1.[36] On the other hand, a single-phase rhombohedral structure was reported by Wu *et al* [37] in NBT-xNN ceramics with x=0.1-0.4, however these researchers did not investigate the impact of electrical poling on crystal structure. The best piezoelectric properties were found for NBT-0.02NN, with d_{33}=80-88 pC N^{-1} and k_p=18 %, but the results of electrostrain measurements were not reported.[36] Another study was focused on both dielectric and impedance analysis for NBT-xNN, but largely ignored compositional effects.[38] Recently, a relative permittivity reaching 1500 over a wide temperature range was reported for NBT-xNN with high NN contents (x=0.4-0.6), which suggests that such compositions might be suitable for use as dielectrics in high temperature capacitor applications. It is also notable that increasing NN content in NBT-NN solid solutions leads to improved dielectric energy storage density up to 0.71 J cm^{-3} at a maximum electric field of 7 kV cm^{-1}, as reported by Xu et al.[7, 39]

The aim of the present study is to precisely determine the impact of electric field on crystal structure and phase transformations in NBT-xNN (x=0.02-0.08) ceramics using high-resolution x-ray powder diffraction (SXPD). Detailed crystallographic parameters are obtained from full-pattern refinements. As reported previously by Wang [22], this was achieved using crushed powders derived from unpoled and poled ceramic pellets to analyse the electric field-induced structural transformations. Microstructure, ferroelectric and piezoelectric properties are investigated alongside crystal structure determination, to provide further insight into the structure-property relationships.

2. Experimental Procedure

$Na_{0.5}Bi_{0.5}TiO_3$-x$NaNbO_3$ (x=0.02, 0.04, 0.06 and 0.08) ceramics were synthesized by the solid-state reaction method using analytical-grade powders: Na_2CO_3(99.8%), Bi_2O_3(99%), TiO_2(99%), Nb_2O_5(99%). Mixed powders were milled for 24 h in propan-2-ol using zirconia milling media, subsequently dried and then calcined for 10 h at 900 °C to form the solid solution. Calcined powders were re-milled for 24 h to break down particle aggregates and reduce particle size. Dried powders were pressed into 6.5 mm diameter pellets under a uniaxial pressure of 150 MPa and sintered at 1180 °C for 3 h in air.

Sintered ceramic samples having a relative density of approximately 95% were finely ground, coated with silver paste (Gwent group) and fired at 500 °C for 30 min to form electrodes. For measurement of ferroelectric properties, the specimens were placed in a silicone oil bath and tested using an electric field up to 6.5 kV mm^{-1} at a frequency of 1 Hz. The amplitude of the electric field was confirmed to be beyond coercive field for NBT-based materials, thereby allowing investigations of the electric field-induced structural transformation. [22, 29, 40-43] Ferroelectric polarisation-electric field loops were recorded using the method described previously.[44] The longitudinal piezoelectric charge coefficient, d_{33}, was measured using a Piezotest PM300 d_{33} meter. Strain-electric field loops were obtained using an aixACCT TF 2000E tester at a frequency of 1 Hz at room temperature. The displacement data was synchronously captured by a laser interferometer. Microstructural examination of the polished cross-sections was carried out by scanning electron microscopy (SEM) using a Phillip XL30. Average grain sizes were determined by the linear intercept method.

Phase identification and structural parameter analysis was achieved by high-resolution

synchrotron x-ray diffraction (SXPD) measurements at beamline I11,[45] Diamond Light Source Ltd., UK. The wavelength of the incident beam (λ=0.494731(10) Å) was calibrated using a diffraction pattern from a high quality Si powder. Unpoled ceramic powders were prepared by crushing as-sintered ceramic pellets, followed by an annealing procedure at 550 °C for 4 h to eliminate residual stress. Poled ceramic pellets were prepared similarly by first removing the conductive electrodes then crushing into fine powder. It was reported previously that such a crushing procedure can be an effective approach to examine electric field-induced structural transformations.[46] The powder samples were loaded and compacted into 0.3 mm diameter glass capillaries, which were mounted onto the spinning capillary holder on the beamline. An energy of 25 keV was used while the diffraction patterns were recorded using a multi-analyser crystal (MAC) detector. Full-pattern refinements of the SXPD patterns were carried out using TOPAS 5.[47] Results of crystallographic parameters and phase fractions were obtained by refinements presented below.

3. Results and Discussions

3.1. Structural characterisation of NBT-xNN (x=0.02-0.08) ceramic powders

All NBT-xNN powders are found to be single-phase perovskite-type solid solutions, as confirmed by the SXPD data. Representative diffraction peak profiles for NBT-xNN powders are presented in Figure 1, showing the $\{111\}_p$, $\{200\}_p$, $\{211\}_p$ and $\{220\}_p$ peak profiles of the 4 compositions for both unpoled and poled powders.

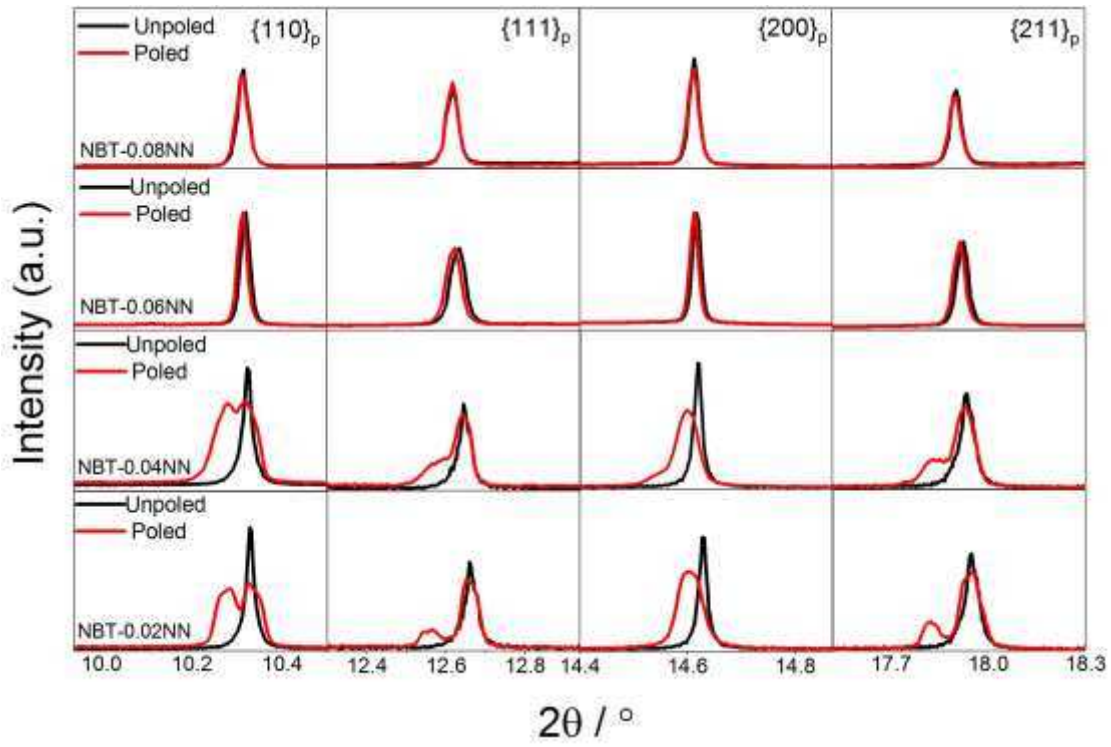

Figure 1. Selected diffraction peak profiles of $\{110\}_p$, $\{111\}_p$, $\{200\}_p$, and $\{211\}_p$ for NBT-xNN powders with x=0.02-0.08, showing both unpoled (black lines) and poled (red lines) states.

For the unpoled state, single peaks are evident for all 4 compositions indicating a predominantly pseudo-cubic structure. All of the peaks shifts to lower angles with increasing NN concentration, indicating an expansion of the lattice. In contrast, for the poled state, peak splitting occurs for x = 0.02 and x = 0.04. Specifically, a rhombohedral phase, characterised by double $\{110\}_p$, $\{111\}_p$, $\{211\}_p$ peaks and a single $\{200\}_p$ peak, are identified for NBT-0.02NN. For NBT-0.04NN, all four peaks are observed to be doublets, indicating a mixed phase of rhombohedral and tetragonal structures. These distorted structures are retained after removing the electric field and crushing the ceramic into powder form prior to the SXPD measurements, indicating the occurrence of an irreversible electric field-induced structural transformation. A similar irreversible field-induced structural transformation from pseudo-cubic to rhombohedral was observed in NBT-xKN (x=0.01-0.05) solid solutions, which was attributed to the nonergodic-relaxor (NR) phase. For

a NR, a pseudo-cubic structure is observed for the unpoled state, which can be transformed into a metastable FE rhombohedral state upon the application of an electric field, which is retained when the electric field is reduced to zero.

It is concluded that the application of an electric field irreversibly transforms the pseudo-cubic phase into a rhombohedral structure, for both NBT-0.02NN and NBT-0.04NN ceramics, indicating their NR nature. In contrast, only slight peak shifts and no peak splitting are evident for NBT-0.06NN and NBT-0.08NN, which comprise a pseudo-cubic phase before and after electrical poling. These observations are attributed to increasing disorder due to the incorporation of NN into the NBT solid solution, as reported in the similar NBT-KN system.[22]

Full-pattern refinement of the diffraction data for NBT-0.02NN and NBT-0.04NN was carried out using TOPAS 5 in order to obtain the crystallographic parameters and quantify the relative phase fractions. For both unpoled and poled powders, experimental diffraction data are fitted using several single or mixed-phase models, such as the rhombohedral *R3m/R3c*, monoclinic *Cc*, tetragonal *P4bm* (weak-polar), *P4mm* and cubic $Pm\bar{3}m$. The best fits for NBT-0.02NN and NBT-0.04NN in the unpoled state are obtained using a single cubic phase, as shown in Figure 2(a-b). The experimental and calculated diffraction patterns are presented in Figure 2(a-b) with representative peak profiles for $\{110\}_p$, $\{111\}_p$ and $\{200\}_p$ and $\{211\}_p$ shown as inserts. The crystallographic parameters determined from the refinements are listed in Table 1 below. In contrast, the best fit for poled NBT-0.02NN is obtained using a single-phase rhombohedral *R3c* structure, as shown in Fig. 2(c), whereas for NBT-0.04NN a mixed-phase refinement comprising rhombohedral *R3c* phase (52%) and tetragonal weak-polar *P4bm* phase (47%) is favoured, as illustrated in Figure 2(d). A significant superlattice diffraction peak, corresponding to the $(\frac{3}{2}\frac{1}{2}\frac{1}{2})_p$

reflection of the *R3c* phase, is also observed for both compositions in the poled state (Figure 2c,d) at a 2θ value of approximately 12.2°, which is related to oxygen octahedral tilting in the *R3c* rhombohedral phase.[48] Additionally, ½(310) at 2θ ~ 16.37078° and ½(510) at 2θ ~ 26.54414°, corresponding to *P4bm* superlattice peaks, are observed for poled NBT-0.04NN. There were no obvious changes in crystal structure for NBT-0.06NN and NBT-0.08NN, which yielded the best fits using a single phase $Pm\bar{3}m$ structure, as shown in Figure S1-2 (supporting information).

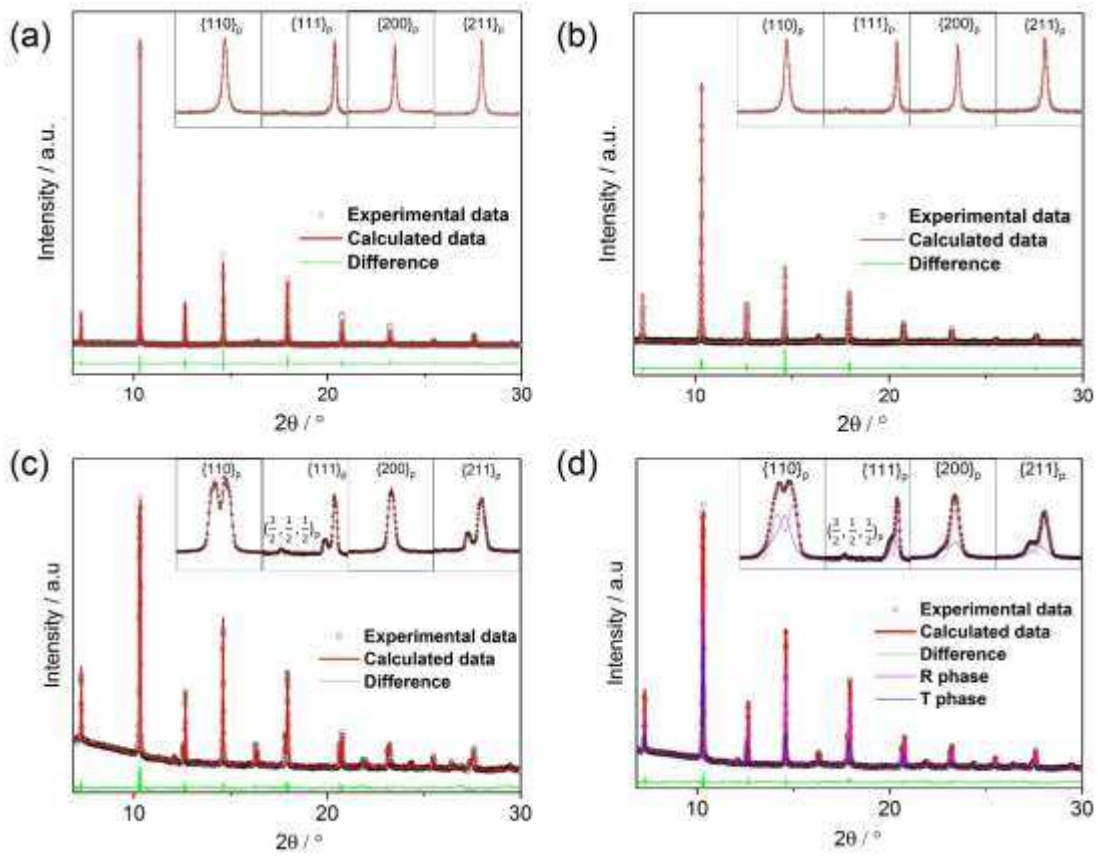

Figure 2. The SXPD full pattern refinements for (a) unpoled NBT-0.02NN, (b) unpoled NBT-0.04NN, (c) poled NBF-0.02NN and (d) poled NBT-0.04NN. The black circles are experimental data, the red line represents the calculated results from the full-pattern refinement, and the green line is the difference profile between experimental and calculated diffraction patterns.

Materials	Phases / %			Lattice parameter					GOF
	R	C	T	R		C	T		
				a / Å	c / Å	a / Å	a / Å	c / Å	
UN-2NN	0	100	0	N/A		3.8806(11)	N/A		1.96
UN-4NN	0	100	0	N/A		3.8825(5)	N/A		1.85
P-2NN	100	0	0	5.4825 (5)	13.5477 (11)	N/A	N/A		2.13
P-4NN	52	0	48	5.4838(3)	13.5394(9)	N/A	5.49654(4)	3.90308(8)	1.87

Table 1. Phase fractions and crystallographic parameters determined from full-pattern refinements for NBT-0.02NN (2NN) and NBT-0.04NN (4NN), in both unpoled (UN) and poled (P) states; R: *R3c*, C: $Pm\bar{3}m$ and T: *P4bm* phase; GOF: Goodness of Fitting.

To facilitate a comparison between the crystal structures of the NBT-NN powders in the unpoled and poled states, the rhombohedral structure is transformed into the equivalent pseudo-cubic setting following the method described previously. [22] The results obtained for the changes in lattice parameter, a_{pc}, and inter-axial angle, α_{pc}, as a function of composition for the NBT-xNN solid solution system are illustrated in Figure 3. For the unpoled state, a single pseudo-cubic phase is identified for all compositions with x=0.02-0.08, while a_{pc} increased from 3.88062(11) to 3.88952(2) Å with increasing NN concentration. The latter trend is consistent with the sizes of the constituent ions, with the estimated effective ionic radius of Na^{+} (1.39 Å) being greater than that of Bi^{3+} (1.03 Å) in 12-fold co-ordination and that of Nb^{5+} (0.64 Å) being greater than that of Ti^{4+} (0.605 Å) in 6-fold co-ordination.[49] During poling of NBT-0.02NN, the structural transformation generates a significant increase of a_{pc}, from ~3.88062(11) Å to 3.89903(7) Å, and reduction of α_{pc}, from ~90.015°(3) to 89.663°(6). For NBT-0.04NN, the application of an

electric field results in significant transformations from a pseudo-cubic phase (a_{pc}~3.88252(5) Å) to mixed rhombohedral (a_{pc}~3.89836(9) Å, α_{pc}~89.697°) and tetragonal (c/a~1.0042) phases.

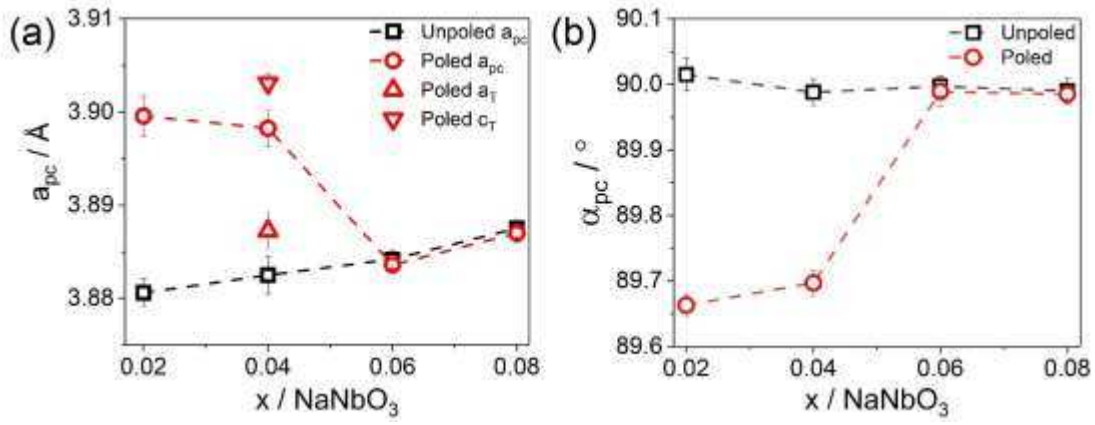

Figure 3. Variations in (a) lattice parameter and (b) inter-axial angle as a function of composition for both unpoled and poled NBT-xNN ceramic powders. The uncertainty in lattice parameters if not shown lies within the size of the data point.

3.2. Polarisation-electric field (P-E) and current density (J-E) loops

The P-E and J-E loops obtained for the NBT-xNN ceramics at room temperature, after poling under an AC electric field of 6.5 kV mm^{-1}, are displayed in Figure 4(a-d). Typical FE switching behaviour is observed for both NBT-0.02NN and NBT-0.04NN at room temperature with high remanent polarization values of approximately 0.24 and 0.28 C m^{-2}, respectively, indicating that an irreversible phase transformation from weak-polar to ordered FE phase had occurred under application of the electric field, denoted as the NR to FE transition.[50] Further evidence can also be found from the appearance of the J-E loops in that a single switching peak is observed at the FE coercive field. This type of irreversible electric field-induced phase transformation was reported previously by Wang and Jo, who observed similar behaviour in NBT-KN and NBT-BT solid solutions.[22, 51] In contrast, the constricted P-E loops, for both NBT-0.06NN and NBT-

0.08NN ceramics, are similar in appearance to those observed in other NBT-based systems.[48, 52] Both of these compositions still exhibit a relatively high maximum polarisation ~0.3 C m^{-2}, but the remanent polarisation values are reduced to approximately 0.2 and 0.1 C m^{-2} respectively. In addition, two peaks are present in the sections of the J-E loops corresponding to both increasing and reducing electric field. This type of behaviour is usually attributed to reversible transformations between weak-polar and metastable long-range ordered FE phases, with the forward and backward transition fields being denoted T_{R-F} and T_{F-R}, respectively. [53] The influence of NN content on the maximum polarisation (P_{max}), remanent polarisation (P_{rem}), E_c and piezoelectric coefficient (d_{33}) for NBT-xNN ceramics are illustrated by the results presented in Figure 4(e, f). The highest values of P_{rem}~0.28 C m^{-2}, P_{max}~0.36 C m^{-2} and d_{33}~118 p CN^{-1} are achieved for the NBT-0.04NN ceramic due to the electric field-induced NR to FE phase transformation and the resulting coexistence of FE rhombohedral and tetragonal phases.

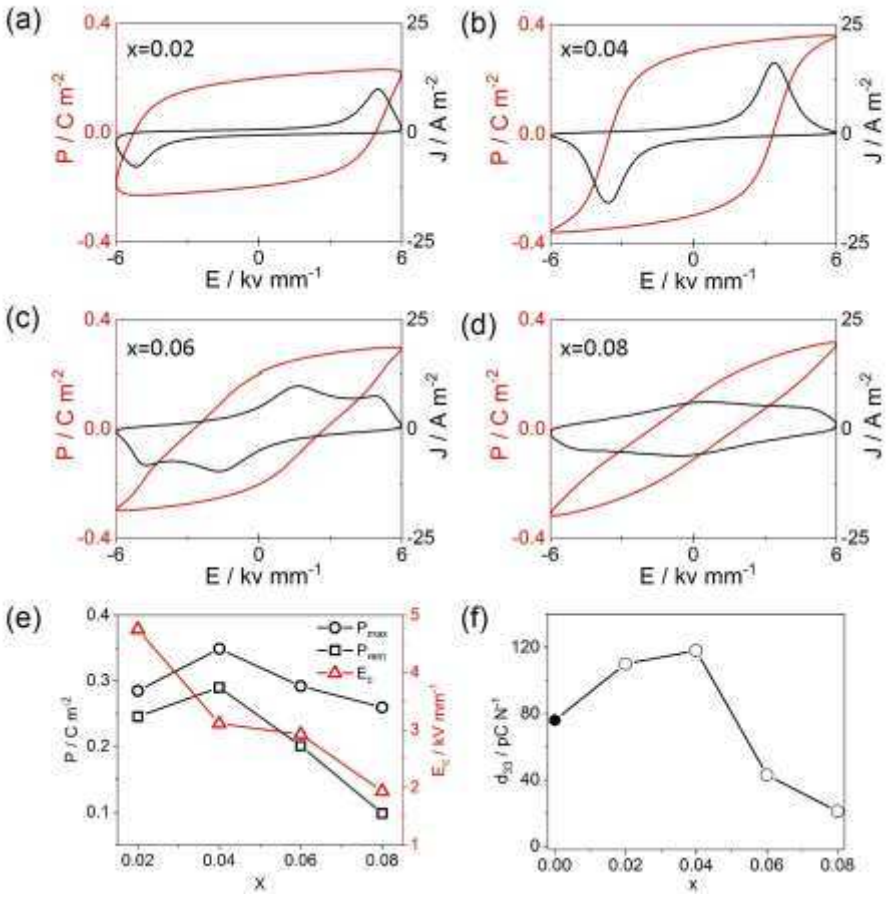

Figure 4. (a-d) P-E and J-E loops (e-f) Variations in P_{max}, P_{rem}, E_c and d_{33} with NN content for NBT-xNN ceramics. *The d_{33} value for x=0.00 was obtained from literature.[36]

3.3. Strain-electric field (S-E) loops

Bipolar and unipolar S-E loops obtained at room temperature for NBT-xNN (x=0.02-0.08) ceramics under an applied electric field of 6.5 kV mm^{-1} are shown in Figure 5. A FE butterfly-type S-E loop is observed for NBT-0.02NN, exhibiting a negative strain (S_{neg}) of ~ -0.08%, saturated strain (S_{sat}) of ~ 0.04% and maximum strain (S_{max}) of ~0.12%. Upon increasing NN concentration to 4%, the magnitude of S_{neg} reduces dramatically while S_{max} nearly doubles, with S_{neg} ~ -0.02%, S_{sat} ~ 0.05% and S_{max} ~ 0.21%. Further increments of NN content led to significant reductions in S_{max} to 0.13% and 0.08%, for NBT-0.06NN and NBT-0.08NN, respectively. Similar behaviour is obtained from unipolar S-E loop, exhibiting S_{max} of ~0.21% for

composition with x=0.04. In summary, the highest S_{max}~0.21% with effective piezoelectric strain coefficient d_{33}^* (=S_{max}/E_{max}) ~343 pm V^{-1} values is obtained for x=0.04, which is attributed to the coexistence of rhombohedral and tetragonal phases.

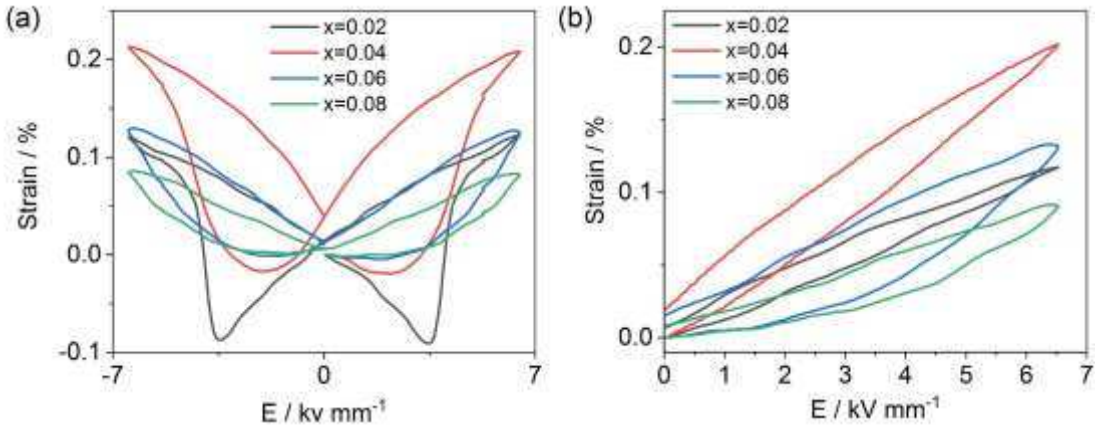

Figure 5. (a) Bipolar and (b) Unipolar S-E loops for NBT-xNN (x=0.02-0.08) ceramics.

3.4. Microstructure of NBT-xNN ceramics

SEM back-scattered electron images from polished cross-sections of NBT-xNN (x=0.02 to 0.08) bulk ceramics are illustrated in Figure 6. The grain size is relatively homogeneous, and no secondary phases were evident for any composition. The average grain size decreases systematically as NN content increases, ranging from ~8.3 μm for x=0.02 to ~5.8 μm for x=0.08. This effect is attributed to the lower diffusion rate for Nb^{5+} ions and the consequent reduction in grain growth rates during high temperature sintering. [54, 55]

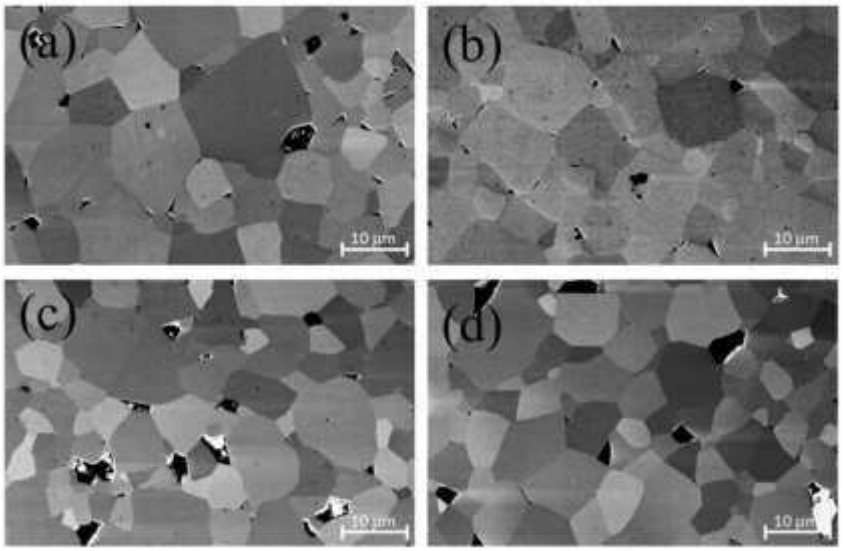

Figure 6. SEM images of polished ceramic cross-sections for (a) NBT-0.02NN (b) NBT-0.04NN (c) NBT-0.06NN (d) NBT-0.08NN.

4. Conclusions

$Na_{0.5}Bi_{0.5}TiO_3$-$xNaNbO_3$ (x=0.02-0.08) ceramics have been successfully synthesized using the solid state reaction method followed by conventional high temperature sintering. An irreversible electric field-induced structural transformation for x=0.02 and x=0.04 is identified using high-resolution SXPD measurements. All compositions in the unpoled state are characterised by a pseudo-cubic structure. Rhombohedral and coexisting rhombohedral-tetragonal phases are observed in poled NBT-0.02NN and NBT-0.04NN ceramics, respectively, while the pseudo-cubic structure is retained for higher NN contents. Similar electric field-induced structural transformations from pseudo-cubic to rhombohedral have been reported for the NBT-KN system. However, higher P_{rem}~0.28 C m^{-2}, S_{max}~0.21%, d_{33}~118 pC N^{-1} and d_{33}^*~343 pm V^{-1} values are obtained for NBT-0.04NN ceramics. Here, we reported that both piezoelectric and ferroelectric properties can be optimized by electric field-induced irreversible structural transformation from nonergodic relaxor ferroelectrics to ferroelectrics, which is critical for

piezoelectric actuator applications.

5. Acknowledgements

The authors are grateful for support provided by Diamond Light Source Ltd under experiment number EE8699.

Reference

[1] Rödel J, Jo W, Seifert KTP, Anton EM, Granzow T, Damjanovic D. Perspective on the Development of Lead-free Piezoceramics. J Am Ceram Soc. 2009;92(6):1153-1177.

[2] Rödel J, Webber KG, Dittmer R, Jo W, Kimura M, Damjanovic D, Transferring lead-free piezoelectric ceramics into application. J Eur Ceram Soc 2015;35(6):1659-1681.

[3] Smolenskii GA, Isupov VA, Agranovskaya AI, Krainik NN, New ferroelectrics of complex composition, Sov Phys Solid State. 1961;2(196):2651.

[4] Huichun Y, Guang Z, Dielectric, ferroelectric, and piezoelectric properties of the lead-free $(1-x)(Na_{0.5}Bi_{0.5})TiO_3$-$xBiAlO_3$ solid solution. Appl Phys Lett 2008;93(11):112902.

[5] Zhang ST, Kounga AB, Aulbach E, Ehrenberg H, Rödel J, Giant strain in lead-free piezoceramics $Bi_{0.5}Na_{0.5}TiO_3$-$BaTiO_3$-$K_{0.5}Na_{0.5}NbO_3$ system. Appl Phys Lett. 2007; 91(11):112906.

[6] Zhang ST, Kounga AB, Aulbach E, Jo W, Granzow T, Ehrenberg H, Rödel J, Lead-free piezoceramics with giant strain in the system $Bi_{0.5}Na_{0.5}TiO_3$-$BaTiO_3$-$K_{0.5}Na_{0.5}NbO_3$. II. Temperature dependent properties. J Appl Phys. 2008;103)3(:034108.

[7] Xu Q, Li T, Hao H, Zhang S, Wang Z, Cao M, Yao Z, Liu H, Enhanced energy storage properties of NaNbO3 modified $Bi_{0.5}Na_{0.5}TiO_3$ based ceramics. J Eur Ceram Soc. 2015; 35(2):545-553.

[8] Wang D, Cao M, Zhang S, Piezoelectric properties of $PbHfO_3$-$PbTiO_3$-$Pb(Mg_{1/3}Nb_{2/3})O_3$ ternary ceramics. Phys Status Solidi RRL. 2012; 6:135-137.

[9] Wang D, Cao M, Zhang S, Piezoelectric ceramics in the $PbSnO_3$-$Pb(Mg_{1/3}Nb_{2/3})O_3$-$PbTiO_3$ ternary system. J Am Ceram Soc. 2011; 94:3690-3693.

[10] Li Y, Wang D, Cao W, Li B, Yuan J, Zhang D, Zhang S, Cao M, Effect of MnO_2 addition on relaxor behavior and electrical properties of PMNST ferroelectric ceramics. Ceram Int. 2015; 41: 9647-9654.

[11] Li Y, Yuan J, Wang D, Zhang D, Jin H, Cao M, Effects of Nb, Mn doping on the Structure, Piezoelectric, and Dielectric Properties of $0.8Pb(Sn_{0.46}Ti_{0.54})O_3$-$0.2Pb(Mg_{1/3}Nb_{2/3})O_3$ Piezoelectric Ceramics. J Am Ceram Soc. 2013; 96: 3440-3447.

[12] Wang D, Cao M, Zhang S, Investigation of ternary system $PbHfO_3$-$PbTiO_3$-$Pb(Mg_{1/3}Nb_{2/3})O_3$ with morphotropic phase boundary compositions. J Am Ceram Soc. 2012; 95: 3220-3228.

[13] Wang D, Cao M, Zhang S, Investigation of ternary system $Pb(Sn,Ti)O_3$-$Pb(Mg_{1/3}Nb_{2/3})O_3$ with morphotropic phase boundary compositions. J Eur Ceram Soc. 2012; 32: 441-448.

[14] Wang D, Cao M, Zhang S, Phase diagram and properties of $Pb(In_{1/2}Nb_{1/2})O_3$-$Pb(Mg_{1/3}Nb_{2/3})O_3$ - $PbTiO_3$ polycrystalline ceramics. J Eur Ceram Soc. 2012; 32: 433-439.

[15] Wang G, Li J, Zhang X, Fan Z, Yang F, Feteira A, Zhou D, Sinclair DC, Ma T, Tan X, Wang D, Reaney IM, Ultrahigh energy storage density lead-free multilayers by controlled electrical homogeneity. Energy Environ Sci. 2019; 12: 582-588.

[16] Wang D, Fan Z, Zhou D, Khesro A, Murakami S, Feteira A, Zhao Q, Tan X, Reaney IM, Bismuth ferrite-based lead free ceramics and multilayers with high recoverable energy density. J Mater Chem A. 2018; 6: 4133-4144.

[17] Wang D, Fan Z, Li W, Zhou D, Feteira A, Wang G, Murakami S, Sun S, Zhao Q, Tan X, Reaney IM, High energy storage density and large strain in $Bi(Zn_{2/3}Nb_{1/3})O_3$-doped $BiFeO_3$-$BaTiO_3$ ceramics. ACS Appl Energy Mater. 2018;1 (8): 4403-4412.

[18] Murakami S, Wang D, Mostaed A, Khesro A, Feteira A, Sinclair DC, Fan Z, Tan X, Reaney IM, High strain (0.4%) $Bi(Mg_{2/3}Nb_{1/3})O_3$-$BaTiO_3$-$BiFeO_3$ lead-free piezoelectric ceramics and multilayers. J Am Ceram Soc. 2018;101: 5428-5442.

[19] Murakami S, Ahmed NTAF, Wang D, Feteira A, Sinclair DC, Reaney IM, Optimising dopants and

properties in $BiMeO_3$ (Me = Al, Ga, Sc, Y, $Mg_{2/3}Nb_{1/3}$, $Zn_{2/3}Nb_{1/3}$, $Zn_{1/2}Ti_{1/2}$) lead-free $BaTiO_3$-$BiFeO_3$ based ceramics for actuator applications. J Eur Ceram Soc. 2018;38: 4220-4231.

[20] Wang D, Khesro A, Murakami S, Feteira A, Zhao Q, Reaney IM, Temperature dependent, large electromechanical strain in Nd-doped $BiFeO_3$-$BaTiO_3$ lead-free ceramics. J Eur Ceram Soc. 2017;37(4): 1857-1860.

[21] Khesro A, Wang D, Hussain F, Sinclair DC, Feteira A, Reaney IM, Temperature stable and fatigue resistant lead-free ceramics for actuators. Appl Phys Lett. 2016;109 (14):142907.

[22] Wang G, Hall DA, Li Y, Murray CA, Tang CC, Structural characterization of the electric field-induced ferroelectric phase in $Na_{0.5}Bi_{0.5}TiO_3$-$KNbO_3$ ceramics. J Eur Ceram Soc. 2016; 36(16):4015-4021.

[23] Daniels JE, Jo W, Rödel J, Jones JL, Electric-field-induced phase transformation at a lead-free morphotropic phase boundary: Case study in a 93%$(Bi_{0.5}Na_{0.5})TiO_3$-7%$BaTiO_3$ piezoelectric ceramic. Appl Phys Lett. 2009;95(3):032904.

[24] Aksel E, Forrester JS, Jones JL, Thomas PA, Page K, Suchomel MR, Monoclinic crystal structure of polycrystalline $Na_{0.5}Bi_{0.5}TiO_3$. Appl Phys Lett. 2011; 98(15):152901.

[25] Levin I, Reaney IM, Nano- and Mesoscale Structure of $Na_{1\backslash2}Bi_{1\backslash2}TiO_3$: A TEM Perspective. Adv Funct Mater. 2012; 22(16):3445-3452.

[26] Chen CS, Chen PY, Tu CS, Polar nanoregions and dielectric properties in high-strain lead-free 0.93$(Bi_{1/2}Na_{1/2})TiO_3$-0.07$BaTiO_3$ piezoelectric single crystals. J Appl Phys. 2014; 115)1(:014105.

[27] Jo W, Granzow T, Aulbach E, Rödel J, Damjanovic D, Origin of the large strain response in $(K_{0.5}Na_{0.5})$ NbO_3-modified $(Bi_{0.5}Na_{0.5})TiO_3$-$BaTiO_3$ lead-free piezoceramics. J Appl Phys. 2009;105)9(:094102.

[28] Royles AJ, Bell AJ, Jephcoat AP, Kleppe AK, Milne SJ, Comyn TP, Electric-field-induced phase switching in the lead free piezoelectric potassium sodium bismuth titanate. Appl Phys Lett. 2010;

97(13):132909.

[29] Wang G, Li Y, Murray CA, Tang CC, Hall DA, Thermally-induced phase transformations in $Na_{0.5}Bi_{0.5}TiO_3$-$KNbO_3$ ceramics. J Am Ceram Soc. 2017; 100(7):3293-3304.

[30] Lanfredi S, Lente MH, Eiras JA, Phase transition at low temperature in $NaNbO_3$ ceramic. Appl Phys Lett. 2002; 80(15):2731.

[31] Cheon CI, Joo HW, Chae KW, Kim JS, Lee SH, Torii S, Kamiyama T, Monoclinic ferroelectric $NaNbO_3$ at room temperature: Crystal structure solved by using super high resolution neutron powder diffraction. Mater Lett. 2015; 156 : 214-219.

[32] Jung JH, Lee M, Hong JI, Ding Y, Chen CY, Chou LJ, Wang ZL, Lead-Free $NaNbO_3$ Nanowires for a High Output Piezoelectric Nanogenerator. ACS Nano. 2011;5(12):10041-10046.

[33] Zhou M, Liang R, Zhou Z, Dong X, Superior energy storage properties and excellent stability of novel $NaNbO_3$-based lead-free ceramics with A-site vacancy obtained via aBi_2O_3 substitution strategy. J Mat Chem A. 2018;6:17896.

[34] Guo Y, Kakimoto KI, Ohsato H, $(Na_{0.5}K_{0.5})NbO_3$-$LiTaO_3$ lead-free piezoelectric ceramics. Mater Lett. 2005; 59(2):241-244.

[35] Lin D, Xiao D, Zhu J, Yu P, Yan H, Li L, Synthesis and piezoelectric properties of lead-free piezoelectric $[Bi_{0.5}(Na_{1-x-y}K_xLi_y)_{0.5}]TiO_3$ ceramics. Mater Lett. 2004; 58(5):615-618.

[36] Li Y, Chen W, Zhou J, Xu Q, Sun H, Xu R, Dielectric and piezoelecrtic properties of lead-free $(Na_{0.5}Bi_{0.5})TiO_3$-$NaNbO_3$ ceramics. Mater Sci Eng B. 2004; 112(1):5-9.

[37] Wu CC, Lin YH, Cheng PS, Chan CC, Yang CF, The Influences of NaNbO3 on the Dielectric and Structure Characteristics of (1-x) $(Na_{0.5}Bi_{0.5})TiO_3$-x$NaNbO_3$ Ceramics. Adv Mater Res. 2012; 415-417 :1064-1069.

[38] Li YM, Chen W, Zhou J, Xu Q, Gu XY, Liao RH, Impedance spectroscopy and dielectric properties of $Na_{0.5}Bi_{0.5}TiO_3$-$NaNbO_3$ ceramics. Physica B: Condensed Matter. 2005; 365(1-4):76-81.

[39] Xu Q, Song Z, Tang W, Hao H, Zhang L, Appiah M, Cao M, Yao Z, He Z, Liu H, Troiler-McKinstry S, Ultra-Wide Temperature Stable Dielectrics Based on $Bi_{0.5}Na_{0.5}TiO_3$-$NaNbO_3$ System. J Am Ceram Soc. 2015;98(10):3119-3126.

[40] Wang G, Hall DA, Comyn TP, Daniel L, Kleppe AK, Structure and ferroelectric behaviour of $Na_{0.5}Bi_{0.5}TiO_3$-$KNbO_3$ ceramics, Adv Appl Ceram. 2016;115(2):89-95.

[41] Fan. Z, Liu. X, Tan. X, Large electrocaloric responses in $[Bi_{1/2}(Na,K)_{1/2}]TiO_3$-based ceramics with giant electro-strains, J Am Ceram Soc. 2017;100:2088-2097.

[42] Fan. Z, Zhou. L, Kim. TH, Zhang. J, Zhang. ST, Tan. X, Mechanisms of enhanced thermal stability of polarization in lead-free $(Bi_{1/2}Na_{1/2})0.94Ba_{0.06}TiO_3$/ZnO ceramic composite, Phys Rev Mater. 2019;3:024402.

[43] Fan. Z, Tan. X, Dual-stimuli in-situ TEM study on the nonergodic/ergodic crossover in the $0.75(Bi_{1/2}Na_{1/2})TiO_3$–$0.25SrTiO_3$ relaxor, Appl. Phys. Lett. (2019), in press.

[44] Hall DA, Stevenson PJ, Mullins TR, Dielectric nonlinearity in hard piezoelectric ceramics, Brit Cer Proc. 1997; 57:197-211.

[45] Thompson SP, Parker JE, Potter J, Hill TP, Birt A, Cobb TM, Yuan F, Tang CC, Beamline I11 at Diamond: A new instrument for high resolution powder diffraction. Rev Sci Instrum. 2009; 80(7):075107.

[46] Garg R, Rao BN, Senyshyn A, Krishna PSR, Ranjan R, Lead-free piezoelectric system $(Na_{0.5}Bi_{0.5})TiO_3$-$BaTiO_3$: Equilibrium structures and irreversible structural transformations driven by electric field and mechanical impact, Phys Rev B. 2013;88:014103.

[47] Diffrac plus TOPAS v. 3.0 (Manual), BRUKER AXS GmbH, Karlsruhe, 2006.

[48] Jo W, Daniels JE, Jones JL, Tan X, Thomas PA, Damjanovic D, Rödel J, Evolving morphotropic phase boundary in lead-free $(Bi_{1/2}Na_{1/2})TiO_3$-$BaTiO_3$ piezoceramics. J Appl Phys. 2011; 109)1(:014110.

[49] Shannon RD, Revised Effective Ionic Radii and Systematic Studies of Interatomic Distances in Halides and Chapcogenides. Acta Crystallogr A. 1976; A32:751.

[50] Viola G, Mkinnon R, Koval V, Adomkevicius A, Dunn S, Yan H, Lithium-Induced Phase Transitions in Lead-Free $Bi_{0.5}Na_{0.5}TiO_3$ Based Ceramics. J Phys Chem C. 2014; 118(16):8564-8570.

[51] Jo W, Schaab S, Sapper E, Schmitt LA, Kleebe HJ, Bell AJ, Rödel J, On the phase identity and its thermal evolution of lead free $(Bi_{1/2}Na_{1/2})TiO_3$-6 mol% $BaTiO_3$. J Appl Phys. 2011; 110)7(:074106.

[52] Sapper E, Schaab S, Jo W, Granzow T, Rödel J, Influence of electric fields on the depolarization temperature of Mn-doped (1-x)$Bi_{1/2}Na_{1/2}TiO_3$-x$BaTiO_3$. J Appl Phys. 2012; 111)1(:014105.

[53] Dittmer R, Lead-Free Piezoceramics Ergodic and Nonergodic Relaxor Ferroelectrics Based on Bismuth Sodium Titanate, University of Darmstadt, 2013.

[54] Swain S, Synthesize and Characterizations of $SrBi_2Ta_2O_9$ Modified NBT-BT and NBT-KNN Ferroelectric Ceramics near Morphotropic Phase Boundary. National Institute of Technology Rourkela, 2015.

[55] Zhao J, Cao M, Wang Z, Xu Q, Zhang L, Yao Z, Hao H, Liu H, Enhancement of energy-storage properties of $K_{0.5}Na_{0.5}NbO_3$ modified $Na_{0.5}Bi_{0.5}TiO_3$-$K_{0.5}Bi_{0.5}TiO_3$ lead-free ceramics. J Mater Sci Mater Electron. 2016; 27(1):466-473.

Captions of all figures

Figure 1. Selected diffraction peak profiles of $\{110\}_p$, $\{111\}_p$, $\{200\}_p$, and $\{211\}_p$ for NBT-xNN powders with x=0.02-0.08, showing both unpoled (black lines) and poled (red lines) states.

Figure 2. The SXPD full pattern refinements for (a) unpoled NBT-0.02NN, (b) unpoled NBT-0.04NN, (c) poled NBF-0.02NN and (d) poled NBT-0.04NN. The black circles are experimental data, the red line represents the calculated results from the full-pattern refinement, and the green line is the difference profile between experimental and calculated diffraction patterns.

Figure 3. Variations in (a) lattice parameter and (b) inter-axial angle as a function of composition for both unpoled and poled NBT-xNN ceramic powders. The uncertainty in lattice parameters if not shown lies within the size of the data point.

Figure 4. (a-d) P-E and J-E loops (e-f) Variations in P_{max}, P_{rem}, E_c and d_{33} with NN content for NBT-xNN ceramics. *The d_{33} value for x=0.00 was obtained from literature.[36]

Figure 5. (a) Bipolar and (b) Unipolar S-E loops for NBT-xNN (x=0.02-0.08) ceramics.

Figure 6. SEM images of polished ceramic cross-sections for (a) NBT-0.02NN (b) NBT-0.04NN (c) NBT-0.06NN (d) NBT-0.08NN.

Captions of all Tables

Table 1. Phase fractions and crystallographic parameters determined from full-pattern refinements for NBT-0.02NN (2NN) and NBT-0.04NN (4NN), in both unpoled (UN) and poled (P) states; R: *R3c*, C: $Pm\bar{3}m$ and T: *P4bm* phase; GOF: Goodness of Fitting.